DOI: 10.1002/adfm.200600651

Solution-Processed Full-Color Polymer Organic Light-Emitting Diode Displays Fabricated by Direct Photolithography**

By *Malte C. Gather*, *Anne Köhnen*, *Aurélie Falcou*, *Heinrich Becker*, and *Klaus Meerholz**

The first full-color polymer organic light-emitting diode (OLED) display is reported, fabricated by a direct photolithography process, that is, a process that allows direct structuring of the electroluminescent layer of the OLED by exposure to UV light. The required photosensitivity is introduced by attaching oxetane side groups to the backbone of red-, green-, and blue-light-emitting polymers. This allows for the use of photolithography to selectively crosslink thin films of these polymers. Hence the solution-based process requires neither an additional etching step, as is the case for conventional photoresist lithography, nor does it rely on the use of prestructured substrates, which are required if ink-jet printing is used to pixilate the emissive layer. The process allows for low-cost display fabrication without sacrificing resolution: Structures with features in the range of 2 μm are obtained by patterning the emitting polymers via UV illumination through an ultrafine shadow mask. Compared to state-of-the-art fluorescent OLEDs, the display prototype (pixel size 200 μm × 600 μm) presented here shows very good efficiency as well as good color saturation for all three colors. The application in solid-state lighting is also possible: Pure white light [Commision Internationale de l'Éclairage (CIE) values of 0.33, 0.33 and color rendering index (CRI) of 76] is obtained at an efficiency of 5 cd A^{-1} by mixing the three colors in the appropriate ratio. For further enhancement of the device efficiency, an additional hole-transport layer (HTL), which is also photo-crosslinkable and therefore suitable to fabricate multilayer devices from solution, is embedded between the anode and the electroluminescent layer.

1. Introduction

Since the first report on efficient electroluminescence from organic materials, organic light-emitting diodes (OLEDs) have been considered as one of the most promising technologies for the next generation of both flat-panel displays and large-area light sources.[1–3] Meanwhile devices based on low-molecular-weight materials are entering the mass market, especially for low-information-content displays in portable devices. Unfortunately, the commonly used processing methods bare some disadvantages for the production of pixilated devices such as displays. Because they are based either on *thermal evaporation*[4] under high vacuum or on *organic vapor-phase deposition* (OVPD)[5] through shadow masks, the methods are relatively expensive, and the achievable resolution is limited to a few tens of micrometers. Furthermore, issues with contact damage and inconsistent pixel sizes are reported as the masks become increasingly overgrown during the evaporation process.

OLEDs based on electroluminescent conjugated polymers are considered as a promising alternative, mainly because of their better compatibility with low-cost production techniques and large substrates. Although polymeric OLEDs have recently seen tremendous advances in performance and lifetime,[6–10] the pixilation of the emissive layer remains one of the key challenges for the production of full-color displays based on electroluminescent polymers.

Various printing techniques have received much attention over the last years, mostly because of their potential for cost-efficient production. Meanwhile several prototypes have impressively demonstrated the feasibility of these methods, especially the ink-jet printing approach.[11–13] However, it was found that these processes can only meet the typical requirements regarding lateral resolution and thickness homogeneity if they are used in combination with substrates that contain a surface-energy template to assists the formation of well-defined pixels with homogeneous surface profiles.[14] So far, these templates were mostly fabricated by a combination of conventional photolithography and plasma exposure, adding at least two additional steps to the production process.

As a consequence, alternative methods for the pixilation of the emissive layer in polymer-based OLED displays were intensively investigated. Because of the ubiquitous presence in the display industry and the high resolutions achievable with this process, conventional photolithography was discussed for

[*] Prof. K. Meerholz, M. C. Gather, A. Köhnen
Institut für Physikalische Chemie, Universität zu Köln
Luxemburgerstr. 116, 50939 Köln (Germany)
E-mail: klaus.meerholz@uni-koeln.de
Dr. A. Falcou, Dr. H. Becker
Merck OLED Materials GmbH
Industrial Park Höchst, F 821, 65926 Frankfurt/Main (Germany)

[**] The authors gratefully acknowledge technical support from Frank Meyer and Junyou Pan (Merck OLED Materials) and from Klaus Mammel (University Ulm). We thank C. David Müller and Nina Riegel for fruitful discussions. The authors acknowledge financial support from the Bundesministerium für Bildung und Forschung (BMBF) through the Hobbit project (13N8952). A. K. also acknowledges financial support from the FCI.

some time.[15–17] However, the incompatibility of the organic materials with the typically water-based processing chemicals was found to reduce device efficiency and lifetime.

Several groups have proposed the use of a thermal imaging process to selectively transfer the emissive material from a donor film to the actual substrate.[18,19] Resolutions in the range of a few tens of micrometers were achieved and full-color displays as well as thin-film-transistor backplanes have been demonstrated. However, to adjust the films strength and to enable clean edge formation, the method requires blending of the emitting polymer with either an inert material such as polystyrene or with a low-molecular-weight hole conductor.

Another alternative is to completely avoid the pixilation of the emissive layer by using either a white-light-emitting polymer in combination with pixilated color filters or interference filters[20] or by employing blue emitters and an array of fluorescent or phosphorescent conversion filters.[21] Although these techniques are in general suited for full-color displays, they will always result in a substantial reduction of device efficiency as a significant fraction of the generated light will be lost in these filters.

Recently, OLED technology has also attracted substantial interest in the area of lighting applications.[2,3] One of the advantages of the use of OLEDs for lighting is the possibility to fabricate devices emitting over a large area, which renders them well suited for diffuse illumination. Again the use of solution-processable polymers might be better suited for large substrates. Although the spectral width of the emission profile of most organic emitters is broad compared to most crystalline inorganic materials, efficient white-light emission is difficult to obtain from a single organic species. Therefore, blend systems and copolymers containing several chromophores emitting in different regions of the visible spectrum are frequently utilized to obtain emission profiles that closely match the white point and have high color-rendering indices.[22–24] Because energy transfer from the sites emitting at short wavelengths (blue part of the spectrum) to sites that are lower in energy, and consequently emit at longer wavelengths, is a very efficient process in this kind of materials, usually low fractions (< 1 %) of red- and green-light-emitting chromophores are sufficient to obtain a balanced emission. However, this often causes strong differential aging and saturation effects at elevated brightness levels, especially for the red-light-emitting species; accordingly, an undesired blue-shift of the emission results. Avoiding this brightness-dependent color-shift has been the focus of intense research over the past years.

In this paper we report on the use of oxetane-functionalized crosslinkable electroluminescent polymers as functional photoresists. We show that these materials are well suited not only to directly define red-, green-, and blue-light-emitting pixels in an OLED display but also to fabricate color-stable and efficient solid-state lighting devices. To start the crosslinking reaction we blended the electroluminescent polymers with small amounts (< 0.5 wt %) of a photoacid that donates a proton upon exposure to UV light. By exposing only certain areas of a thin polymer film (for example through a shadow mask), we were able to selectively crosslink the films. Since the crosslinking process renders the films insoluble, rinsing the films with an organic solvent dissolves only the unexposed (i.e., non-crosslinked) regions of the film. Thus, these materials effectively work as negative photoresists, and thin films of these polymers can be directly structured via photolithography. We believe that this technique is a very promising alternative to the approaches that are currently discussed in the literature for structuring the emissive layer of OLED displays.

In our previous work we have used the photoinitiated oxetane-based crosslinking reaction to fabricate insoluble triphenylamine-dimer (TPD) hole-injection layers and have demonstrated solution-processed multilayer OLEDs with improved device efficiency based on this approach.[6,25,26] Recently, we also reported on photo-crosslinkable electroluminescent polymers and developed a crosslinking procedure that does not have a negative impact on the performance of the final device, which is remarkable given the sensitivity of electroluminescent polymers to chemical modifications and impurities.[27]

Here we present a fully operational red–green–blue (RGB) display based on electroluminescent polymers, which are directly structured via photolithography. We demonstrate that display resolutions far in excess of 1000 pixels per inch (ppi) are feasible with the proposed patterning process. With slight modifications, the device structure was also used to fabricate lighting devices. The emission profile of these devices can be set to any color within a large color gamut and is maintained over several orders of magnitude in brightness by a simple but efficient adaptation system. As an example we discuss the device characteristics for the case of white emission (Commision Internationale de l'Éclairage (CIE) 0.33, 0.33) and find that pure white light can be obtained with a current efficiency of 5 cd A^{-1}.

2. Results and Discussion

2.1. Materials System

To implement the photoresist properties, the emitter polymers (Fig. 1 and Table 1) used in this work contain oxetane moieties that are attached to the polymer backbone via an alkyl spacer. Compared to other crosslinking routes discussed in the literature, the oxetane crosslinking reaction has several ad-

Table 1. Composition of the polymers **BX**, **GX**, and **RX**.

Monomer	**BX** [a] [mol %]	**GX** [a] [mol %]	**RX** [a] [mol %]
1	50	50	50
2	25	15	10
3	15	–	–
4	10	10	10
5	–	25	–
6	–	–	5
7	–	–	25

[a] Monomer feed ratio [mol %] for the polymerization (see Fig. 1).

ADVANCED FUNCTIONAL MATERIALS

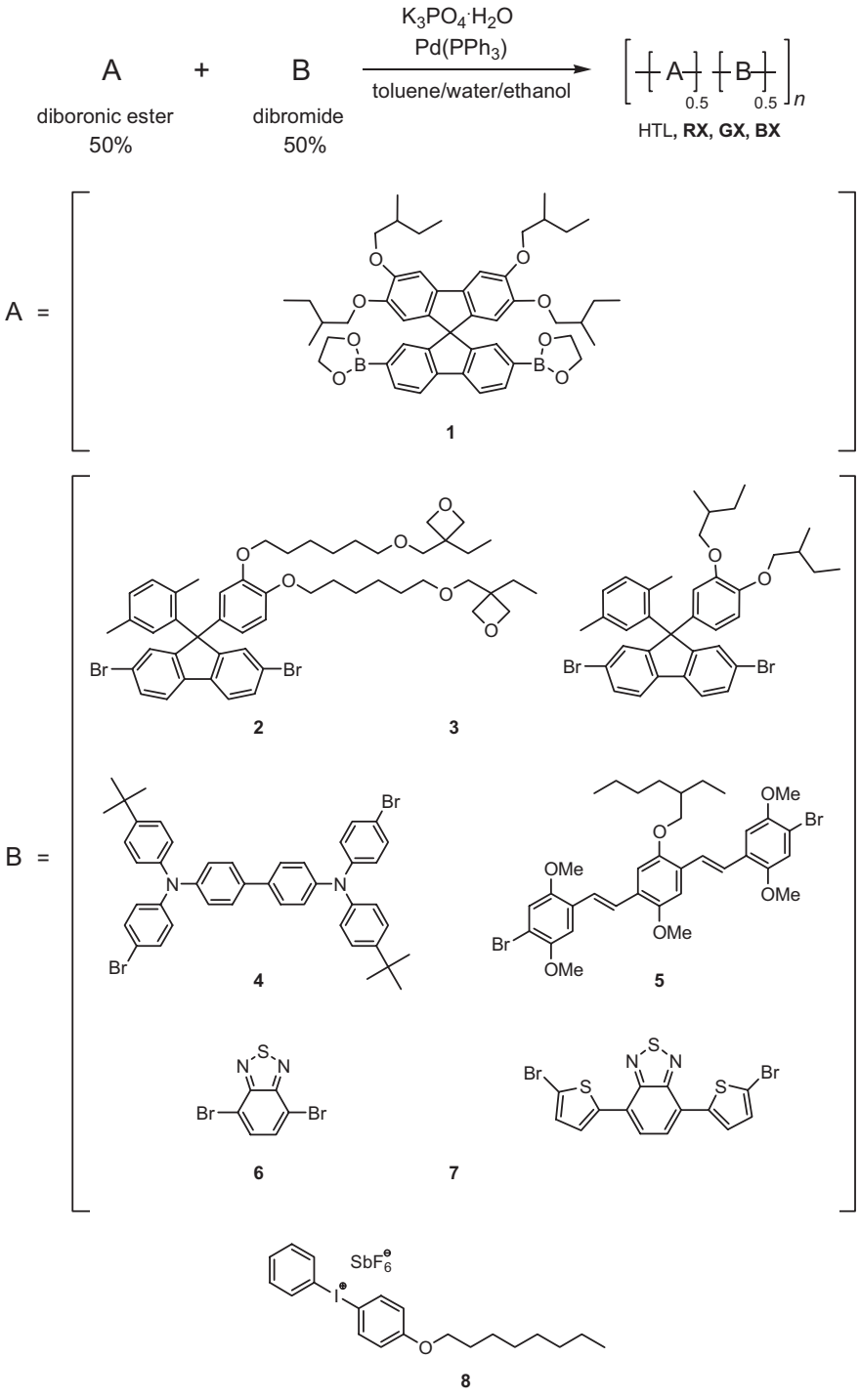

Figure 1. General scheme for synthesis of the polymers **RX**, **BX**, **GX** (top), chemical structure of monomers **1**–**7** (middle) and chemical structure of the photoacid **8** (bottom).

vantages such as small volume shrinkage, no inhibition by the presence of oxygen, compatibility with the strongly basic conditions of transition-metal-catalyzed coupling reactions, and negligible modification of the electrical and optical properties of the material.[28–30] All polymers were copolymers, containing the monomer **2,** to which the oxetane functionality is attached. For the green- and red-light-emitting polymers, chromophores emitting in the respective wavelength region were also copolymerized into the polymer chain. The blue polymer possesses 25 mol % of the oxetane substituted monomer **2**. The green one contains 15 mol % and the red one only 10 mol %. In the following the polymers will be referred to as **RX**, **GX**, and **BX**, respectively. For the general synthesis of these copolymers, which are similar to the polymers used in our previous work, see Figure 1.[27]

The chemical structure of the photoacid (**8**), which is added to the polymer solutions to initiate the crosslinking process, and the mechanism of the cationic ring-opening polymerization (CROP) of the oxetane units are shown in Figures 1 and 2, respectively. Like many other photoreactions, CROP is sensitized by the presence of aromatic moieties. In our case, this is the π-system forming the polymer backbone, which means that sensitization is very efficient because of the high number density of aromatic units (essentially the entire material) and because of their high absorption cross section. Illumination leads to highly efficient photoinduced electron transfer (PET) to the photoacid, ultimately yielding radical cation sites on the emissive polymer.[31,32]

2.2. Process Development

We began our investigations by optimizing the different parameters affecting the crosslinking properties and the resolution of the direct photolithography process. Because the polymer films remain soluble after UV irradiation, a soft-curing step is required to promote the crosslinking. The heat allows for sufficient rotational diffusion of the oxetane side groups and thus increases the crosslinking rate, ultimately making the material insoluble.[27] (The soft-curing temperatures are in the range of 60–90 °C.) Finally, after rinsing the films, an additional post-curing step (200 °C) is needed to destroy the radical cations that are left from the PET. One can not merge these two curing steps to one at 200 °C before developing the film because the high temperature would lead to undesired crosslinking in the non-illuminated regions of the film. This results from the fact that CROP is a living polymerization without a specific termination step. Crosslinking is only terminated when the emerging network inhibits the rotational diffusion of the oxetane side groups as the reaction proceeds. Diffusion pro-

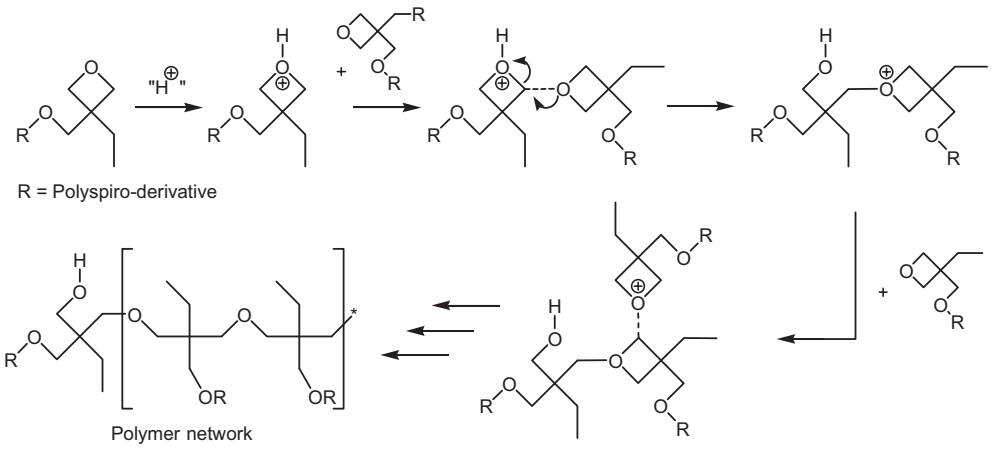

Figure 2. Illustration of the cationic ring-opening polymerization (CROP) of oxetanes. The proton, which is generated photochemically, initiates the reaction by activating one oxetane ring for the nucleophilic attack of a second oxetane ring. The first ring then opens, leaving the second ring activated. A third ring can attack and so on, until a 3D network is formed.

cesses can therefore cause crosslinking of the polymer in unexposed parts of the films, if not controlled properly.

As discussed above, the resolution of a patterning process is often the critical factor regarding the application of certain lithographic or printing technologies for display production. To quantify the resolution, we irradiated spin-cast films of the crosslinkable polymers through a shadow mask with varying feature size (US Air Force (USAF) 1951 resolution target structure, see Experimental). In various test runs, the concentration of the oxetane groups in the polymer, the concentration of the photoacid, the UV exposure dose, and the soft-curing temperature were identified as the parameters with the most significant impact on the process resolution. In general, the tendency for an undesired crosslinking in non-exposed regions of the sample was larger for polymers with more oxetane groups and for blends with high concentration of photoacid. Long exposure times and high soft-curing temperatures had a similar effect. Conversely, reducing the oxetane and photoacid concentration, the exposure time, and the curing-temperature below a certain value led to incomplete crosslinking. As an example, Figure 3 shows the influence of the soft-curing temperature: For high curing temperatures ($T_C = 90\,^{\circ}C$), structures below 40 μm in size are no longer resolved with full modulation. However, as the curing temperature was gradually reduced ($T_C = 75$ and $60\,^{\circ}C$), even the finest structures of the USAF target, which have a line width of 2 μm, were resolved with full modulation, i.e., there was no crosslinking between adjacent stripes. Note that with holographic methods, even higher resolutions were demonstrated with similar material systems.[31] If the curing temperature was reduced even further, the exposed areas of the films were still partly soluble and a substantial loss in film thickness was observed during the development step.

We would like to emphasize that very low radiation doses ($< 10\ \mu J\,cm^{-2}$) were found to be sufficient to initiate the crosslinking reaction. This results from the very efficient photosensitization of the CROP reaction via PET.

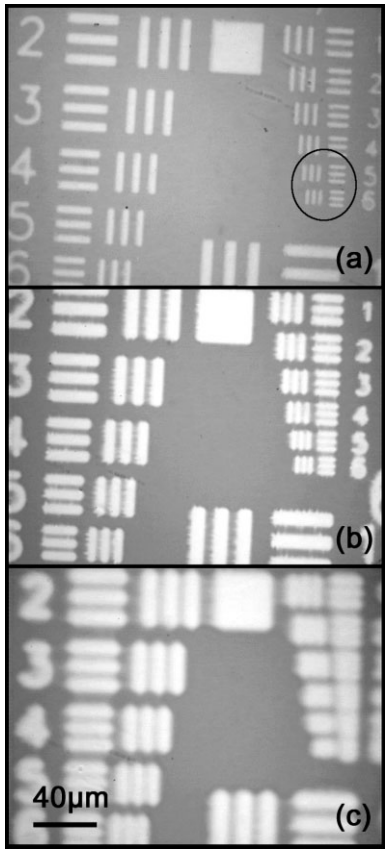

Figure 3. Influence of the soft-curing temperature on the resolution of the direct lithography process. The microscopy images show thin films (60 nm thickness) of the green emitter (**GX**, containing 0.5 wt% of the photoacid **8**) patterned by contact lithography. The films were exposed to UV light for 30 ms (corresponding to a radiation dose of 200 $\mu J\,cm^{-2}$) through a USAF 1951 resolution test mask and soft-cured at a) 60 °C, b) 75 °C, and c) 90 °C before they were developed by spin-rinsing with tetrahydrofuran (THF). In (a), the smallest features of the resolution target (ca. 2 μm, see features marked with circles) are resolved with full modulation.

ADVANCED FUNCTIONAL MATERIALS

2.3. Device Fabrication

After having systematically studied the process parameters influencing the direct lithography process, a simple passive matrix display was fabricated (referred to as Device A). The pixels of the prototype display have the following general device structure: ITO/PEDOT:PSS (35 nm)/HTL (20 nm)/EL polymer/Ba (4 nm)/Ag (150 nm) (ITO: indium tin oxide, PEDOT: poly(3,4-ethylenedioxythiophene), PSS: poly(styrenesulfonate) HTL: hole-transport layer, EL: electroluminescent layer).

The general fabrication procedure was as follows (also see Fig. 4): The PEDOT layer and a layer of a crosslinkable triarylamine-based hole conductor (HTL) were deposited on top of a structured ITO anode (structured via conventional photolithography and wet etching, ITO line width 200 µm, spacing 100 µm). In the next step, the first electroluminescent polymer (**BX**) was spin-coated on top of the HTL layer and then illuminated with UV light through a shadow mask to start the crosslinking reaction of the oxetane units. After soft-curing, the non-illuminated areas remained soluble and were washed off with tetrahydrofuran (THF). The deposition, crosslinking, and development steps were repeated for the **GX** and the **RX** polymers, so that eventually 300 µm wide stripes of the three different polymers were aligned parallel to each other. The layer thickness was 70 nm for **GX**, 95 nm for **RX**, and 80 nm for **BX**. Before the evaporation of the cathode, the devices were post-cured at 200 °C. In the final step, cathode stripes were evaporated perpendicularly to the polymer stripes (shadow mask line width 600 µm, spacing 300 µm) to form the passive matrix structure.

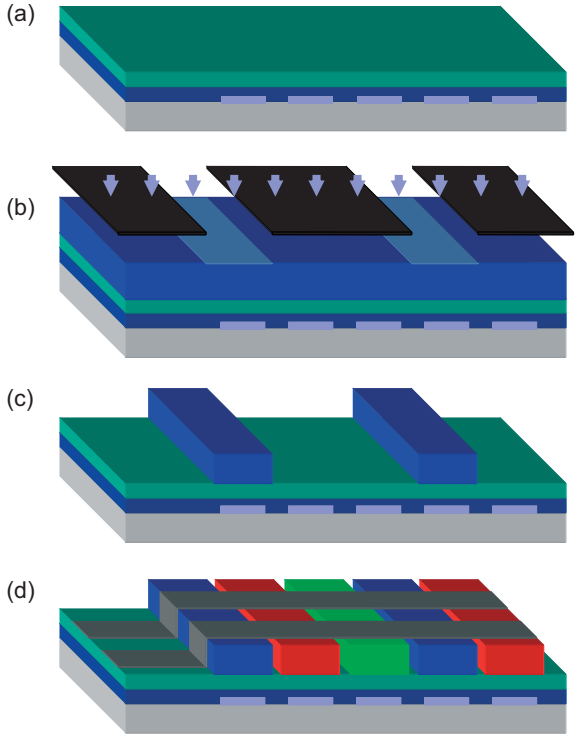

Figure 4. Schematic illustration of the direct lithography process: a) On top of an ITO line structure, homogenous layers of PEDOT:PSS and a crosslinkable hole-transport material are spin-coated. b) Subsequently, a solution of the blue-light-emitting polymer is deposited and exposed to UV light through an aligned shadow mask. c) After a soft-curing step, the non-crosslinked parts are dissolved in an organic solvent. Repeating this procedure for **GX** and **RX** results in parallel stripes of blue-, green-, and red-emitting polymers. d) The device is completed by evaporating a metal cathode through a shadow mask.

The precise alignment of the different polymer stripes with the ITO anode was confirmed with an optical microscope and by surface profilometry (Fig. 5). The electroluminescent area of one subpixel, which is defined by the overlap of the ITO anode and the cathode, measures 200 µm × 600 µm. Because of the spacing between the adjacent columns and rows, one full RGB pixel covers an area of 900 µm × 900 µm resulting in a fill factor of about 44 %. Using 36 pixels × 20 pixels, the total display covers an area of 18 mm × 11 mm.

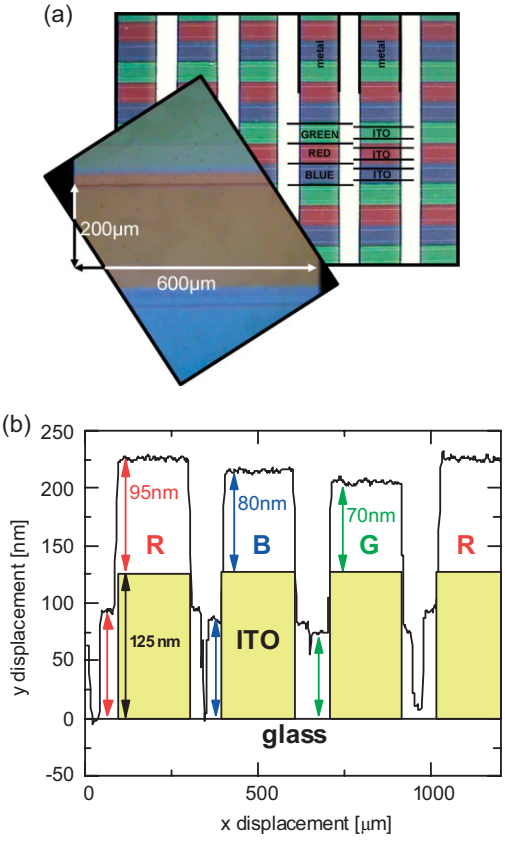

Figure 5. a) Microscopy image of the completed display taken through the glass substrate. The horizontal polymer stripes are parallel and well-aligned with the underlying ITO anode stripes. The metal cathode columns are seen as vertical stripes. (The separating white stripes result from the microscope backlight overexposing the camera.) The inset shows a single RGB triple at a higher magnification. b) Profilometric scan of the device surface taken perpendicular to the polymer stripes. The arrows and the yellow boxes indicate the contribution of the ITO layer and of the respective polymer layer to the total layer thickness.

2.4. Device Testing

The displays were characterized by measuring the current–voltage–luminance (*I*–*V*–*L*) characteristics (Fig. 6). To reduce the experimental error involved in the low absolute brightness

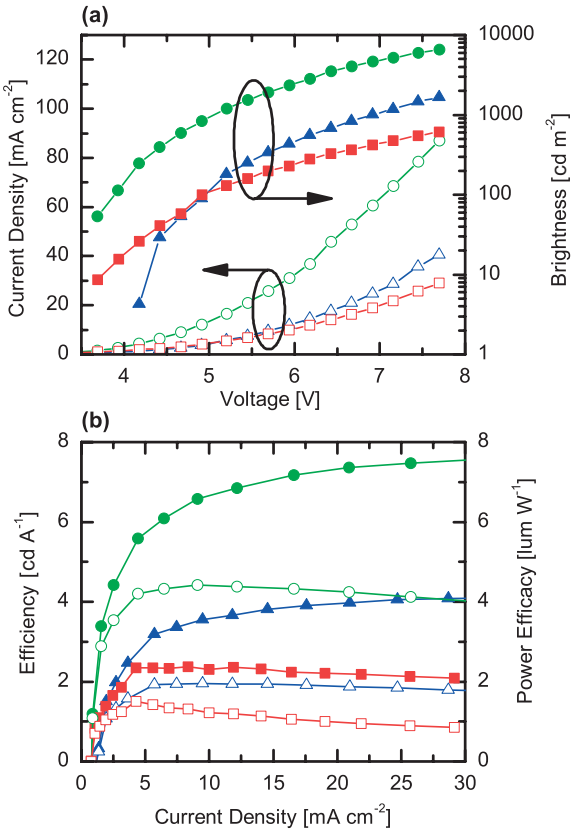

Figure 6. a) Current–voltage–luminescence characteristics of individual columns of red (■, □), green (●, ○), and blue (▲, △) emitting pixels in Device A. Open symbols display the current density, closed symbols display the brightness versus applied voltage. b) Efficiency (filled symbols) and power efficacy (open symbols) versus the current density calculated from the *I–V–L* curves in (a).

levels emitted from single pixels, the data were taken for a full column of pixels for each color. The variation between different lines of the same color was negligible, as discussed below (see also Fig. 10). Although the lithographic structuring of the emissive layer was done in air, the device efficiency was improved compared to our previous work.[27] This mainly results from the additional HTL layer.[25] We also observed an improvement compared to reference OLEDs with an unstructured emissive layer but with the same device structure and processing parameters (Tables 2 and 3). We attribute this to the use of a smaller emissive area, which reduces the heating of the devices (0.12 mm^2 for one pixel instead of 8 mm^2 for the reference samples). This reduction in device heating also results in a less steep reduction of efficiency with increasing voltage for all three colors. As an example, Figure 7 summarizes the efficiency of all green-light-emitting display and reference devices (also compare Tables 2 and 3). One can clearly see that, for the display, the drop in efficiency with increasing voltage is less pronounced than for all reference devices. The corresponding efficiency for reference devices (emissive area 8 mm^2) processed under nitrogen and for reference devices with non-crosslinked emissive layers (processed under air and

Table 2. Characteristics of the two device types structured by direct photolithography.

	BX	GX	RX
Device A (20 nm HTL)			
Thickness of emissive layer [nm]	80	70	95
η_{max} [cd/A] [a]	4.1	7.7	2.3
CIE (x,y) [b]	(0.153, 0.155)	(0.310, 0.606)	(0.676, 0.324)
Device B (40 nm HTL)			
Thickness of emissive layer [nm]	60	60	60
η_{max} [cd/A]	6.5	7.9	2.5
CIE (x,y)	(0.255, 0.287)	(0.349, 0.541)	(0.670, 0.328)

[a] η_{max}: maximum current efficiency; [b] CIE (x,y): color coordinates according to the 1931 CIE standard.

Table 3. Efficiency data of the different reference devices (active area 8 mm^2) discussed in the article.

		BX	GX	RX
Thickness of emissive layer [nm]		80	70	95
η_{max} [cd/A]	x-linked (air) [a]	2.5	5.3	1.4
	x-linked (N_2) [a]	2.7	6	–
	pristine (air) [a]	2.9	6.5	1.4
	pristine (N_2) [a]	2.9	8.2	1.4

[a] "x-linked" refers to crosslinked and nonstructured devices; "pristine" refers to noncrosslinked and nonstructured devices without addition of photoacid **8**; "air" refers to fabrication under the same condition as used for the display (spin-coating, crosslinking and soft-curing under air); "N_2" refers to spin-coating, crosslinking and soft-curing under a nitrogen atmosphere in the glove-box system.

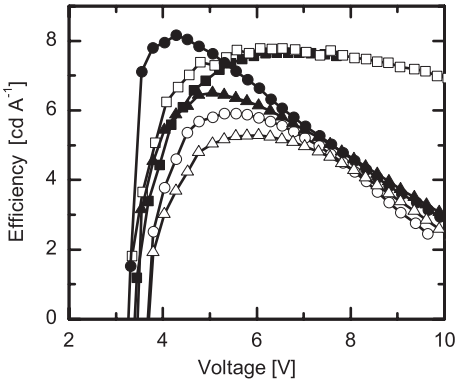

Figure 7. Comparison of the efficiency of the different green-emitting devices: Device A with 20 nm HTL and 70 nm EL (■); Device B with 40 nm HTL and 60 nm EL (□); reference device pristine, processed in N_2 (●); reference crosslinked, processed in N_2 (○); reference pristine, processed in air (▲), reference crosslinked, processed in air (△). For more information see footnote to Table 3.

under nitrogen) is also shown in Table 3. For **RX**, the crosslinking reaction shows almost no effect on efficiency, whereas a small reduction in efficiency was observed for **GX** and **BX**. We believe that despite the thorough post-curing process, some radical cations remain in the polymer film. These constitute nonradiative recombination sites, which lie energetically in be-

ADVANCED FUNCTIONAL MATERIALS

tween the radiative transitions of the green- and the red-light-emitting polymers, as confirmed by time-resolved fluorescence spectroscopy. Processing the polymers in air also reduces the device efficiency, especially for the green-light-emitting polymer, but mainly affects the device lifetime.

The extrapolated half-brightness lifetime at an initial brightness of 100 cd m^{-2} is in the range of 100 h for **BX**. Although this result is clearly not satisfactory for display applications, we have recently achieved lifetimes >1000 h at 100 cd m^{-2} with a modified blue-light-emitting crosslinked polymer. Further details will be published elsewhere. We also note that the lifetime measurements reported here are based on a DC driving scheme. By using pulsed AC driving with a reverse bias voltage component, a further improvement of the device lifetime is expected.[33]

For display applications, the color saturation of the red, green, and blue primaries is an important factor. Even if the different emitters show well-saturated emission spectra, when used in nonstructured reference devices, significant "color contamination" may occur; for example, if a small amount of the red-light-emitting polymer is mixed into the blue-light-emitting material. Therefore, the EL spectra and the CIE values of the different polymers were measured in the final device (for single subpixels). We observed pure emission from each color as long as the three emitters were deposited in the correct sequence, i.e., **BX** deposited first, **GX** second, and **RX** at the end (see Fig. 8). These results are in contrast to our earlier work, where we found that the deposition sequence of the three polymers had no influence on the EL spectra.[27] We believe that this is because of the smaller pixel sizes we used for the display reported here.

After this basic characterization, the devices were connected to a commercial passive-matrix controller operating in pulsed-current mode, which allowed us to address each pixel separately (see Experimental for details).[34] We obtained a homogenous brightness level across the entire device and were able to display various test pictures and animations (see Fig. 9). We note that, as expected from simple resistance estimations, there is no crosstalk between adjacent columns. By using pulse width modulation, up to 256 gray levels were accessible for each color.

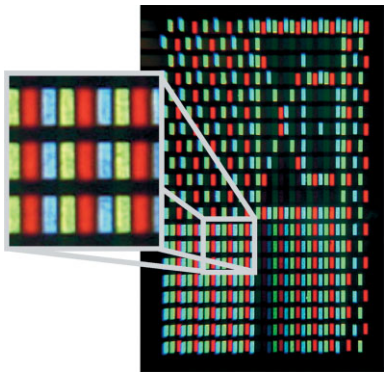

Figure 9. Photograph of the operating display showing a test screen. No crosstalk is observed between adjacent rows and columns, and uniform brightness is achieved across the entire device. In the lower right corner the brightness of the pixels was varied by means of pulse-width variation. The apparent vertical offset between the red, green, and blue pixels in the upper and lower part of the picture results from aberration effects of the camera objective.

For display applications, it is important to maintain a constant thickness of the emissive layer across the entire device, as thickness variations result in brightness inhomogeneities and differential aging. Such variations can be caused, for example, by particle contamination during the spin-coating process. As a simple but effective method to study pixel-to-pixel deviations and also to detect pixel defects, we determined the voltage that is necessary to drive each pixel at a predefined current (in this case a current pulse of 180 μA, corresponding to 150 mA cm^{-2}). Figure 10 shows a map of the deviation from the median voltage for a typical device, that is, the average (median) driving voltage for each color has been subtracted from the measured values to allow for an easier identification of any inhomogeneities. One defective (short) pixel (Defect 1) and an area of increased operating voltage (Defect 2) can be

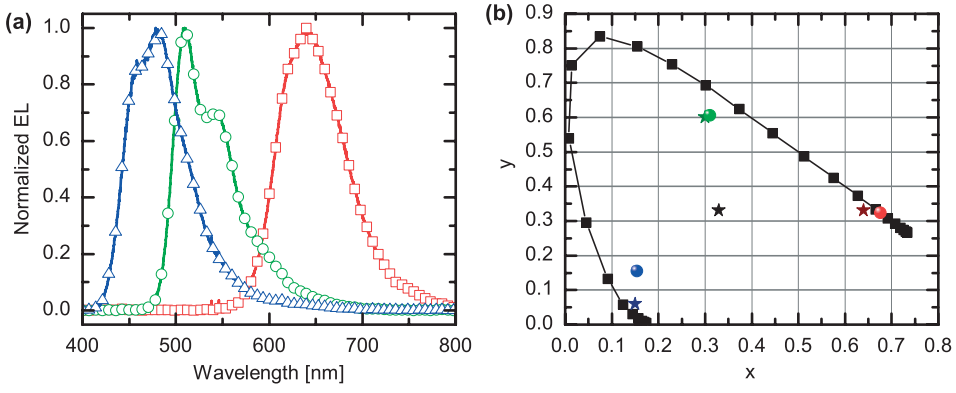

Figure 8. a) EL spectra measured for single pixels of each color of Device A: red pixel (□), green pixel (○), and blue pixel (△). All spectra were color-stable between 100 cd m^{-2} and 1000 cd m^{-2}, that is, the shape of the EL spectrum remained unchanged within the resolution of the spectrometer and the variation of the CIE coordinates derived from the spectra was below 0.004. b) CIE coordinates calculated from the EL spectra shown in (a). The values for the display colors are depicted as balls, whereas the stars show the cathode ray tube (CRT) standard CIE values as well as the white point (0.33, 0.33).

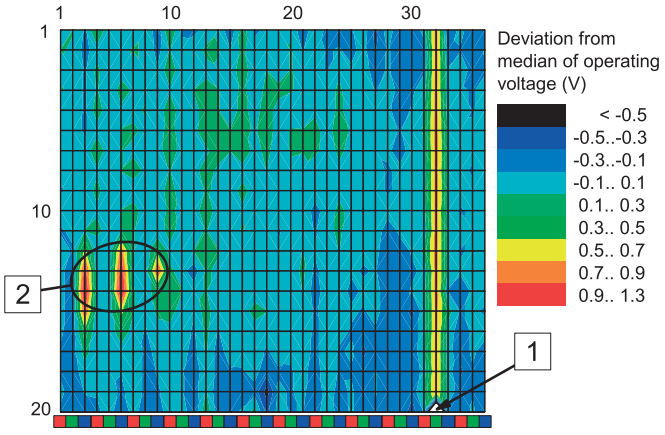

Figure 10. Map of the voltage applied to each pixel at a (pulsed) driving current of 180 μA (corresponding to 150 mA cm^{-2}). The color code at the bottom indicates the emission color of the respective columns. The average bias voltage (median) for each color (red: 7.26 V, green: 5.76 V, blue: 7.07 V) was subtracted. The areas marked "1" and "2" are discussed in the text.

clearly identified in the voltage map. Both result from comet tails in the emissive layer caused by particle contamination (as confirmed via optical inspection). The voltage variation in the area of Defect 2 is limited to the layer deposited first (polymer **BX**), confirming that there is no influence of the underlying structures on the homogeneity of polymer films deposited afterwards. This is also confirmed by surface profilometry (Fig. 5). We point out that for the rest of the display area the voltage difference between pixels of the same color is below 3 %, indicating that the direct lithography process does not have a negative impact on the thickness homogeneity of the spin-coated films. (The increased operating voltage of the pixels in the column containing Defect 1 results from an artifact of the driver electronics: The positive row voltage under which all inactive cathode rows are kept during the measurement adds to the measured operating voltage because the row and the column containing the defective pixel are interconnected.) Also note that, despite rather poor clean room conditions present during device fabrication and although we used contact lithography, the error rate, that is, the fraction of defect pixels per total number of pixels, in the final devices was only ca. 10^{-3}. We believe that under state-of-the-art clean-room conditions and by using noncontact lithography, an error rate compatible with industrial requirements can be easily achieved.

2.5. White-Light Emission

OLEDs with a white-light emission spectrum are currently the focus of intense research.[1–3] An alternative to the copolymer and blend systems, which are currently being investigated, could be to use red-, green-, and blue-light-emitting devices positioned in close proximity. While this method has proven very successful for inorganic LEDs, there are only few adaptations to organic systems.[35] One of the main advantages of devices containing separately addressable red-, green-, and blue-light emitters is that the color coordinates of light emitted by the whole device can be adjusted within a color gamut defined by the three primaries. Therefore, such devices can not only be used for general lighting applications, but also as mood-lighting panels as well as allow for active compensation of any differential color aging.

Because the materials used in this work (especially the green- and blue-light-emitting materials) show reasonable device performance, one might want to consider them for such applications. In the following we calculate how efficient light of a certain color can be generated.

The total brightness (Y, in cd m^{-2}) emitted by our devices is given by the average of the three brightness levels:

$$Y = (Y_R + Y_G + Y_B)/3 \tag{1}$$

It can be easily shown that the CIE coordinates of the light emitted by the whole device are given by the following expression:

$$(x, y) = \left(\frac{\sum_{RGB} x_i Y_i / y_i}{\sum_{RGB} Y_i / y_i}, \frac{\sum_{RGB} Y_i}{\sum_{RGB} Y_i / y_i} \right) \tag{2}$$

where, x_i and y_i denote the CIE coordinates of the three primaries and Y_i their respective brightness level. If the CIE coordinates of the primaries are known, this equation can be analytically solved for Y_i. For example, to obtain white light (CIE coordinates of $x = 0.33$, $y = 0.33$) and using the CIE coordinates of the three emitters, the resulting brightness ratio of red/green/blue is 27:53:20. Using spline fits to describe the functional dependence between current density (j_i), luminescence (Y_i), and voltage (U_i) for all three emitters (i = R,G,B), one can directly calculate the current density and the operating voltage for each of the emitters as a function of the overall brightness level Y. The total current density j_{total}, and hence, the total current efficiency η_{total} are obtained by adding the current densities, as given in Equations 3 and 4, respectively.

$$j_{total}(Y) = \sum_{RGB} j_i(Y) \tag{3}$$

$$\eta_{total}(Y) = Y / j_{total} \tag{4}$$

Finally, assuming Lambertian emission characteristics, the total power efficiency η_P is given as a function of the total brightness

$$\eta_P(Y) = \frac{Y \times \pi}{\sum_{RGB} j_i(Y) \times U_i(Y)} \tag{5}$$

We calculated η_{total} and η_P from the I–V–L characteristics for a slightly modified device structure (referred to as Device B) that was optimized for efficiency rather than for color purity. Device B was fabricated by depositing the emitters in reverse sequence, that is, **RX** then **GX** and finally **BX**, and by using an optimized layer arrangement of the HTL and the EL layer.

ADVANCED FUNCTIONAL MATERIALS

The general device structure is then ITO/PEDOT:PSS (35 nm)/HTL (40 nm)/EL polymer (60 nm)/Ba (4 nm)/Ag (150 nm). Such a device shows improved efficiency for the individual colors but shifted CIE coordinates relative to previous devices (see Table 2). The surprisingly high efficiency for **BX** in Device B compared to Device A mainly results from the color shift to a less saturated blue. Using Equations 4 and 5, a peak current efficiency and power efficacy of 5 cd A^{-1} and 3.5 lm W^{-1}, respectively, is obtained for pure white light (CIE: 0.33, 0.33) (see Fig. 11).

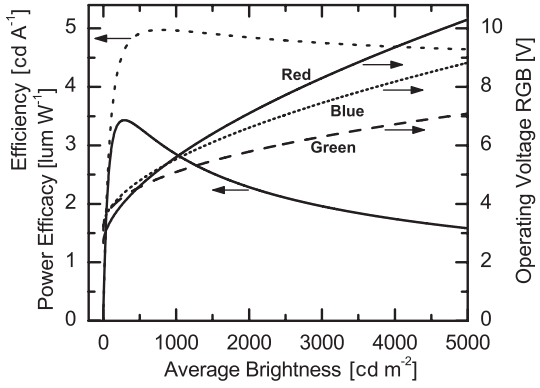

Figure 11. Left axis: Power efficacy (solid line) and current efficiency (short-dashed line) of Device B for the emission of white light (CIE 0.33, 0.33) calculated from experimental data using Equations 4 and 5. Right axis: The bias voltage which has to be applied to the red (solid), green (dashed), and blue (dotted) emitters to achieve a corresponding average brightness level of white emission as shown on the *x*-axis.

3. Conclusions

Electroluminescent polymers with photoresist-like properties are a new and promising alternative for the fabrication of low-cost polymer OLED displays. Because of the possibility to directly structure the luminescent polymer layer, this requires fewer fabrication steps than competing technologies. The process is solution-based and does not require additional substrate or equipment preparation.

The manufactured prototype shows very good *I–V–L* characteristics, as well as good color saturation for all three polymers. In comparison with nonstructured OLEDs, no significant decrease in the efficiency was observed.

The characteristic size of the created structures is not limited by the crosslinking properties of the polymers itself (structures beyond 2 μm were obtained), but by the resolution of the lithography masks used in this work. On an industrial scale, it seems feasible to fabricate displays with very high resolutions and to reduce the spacing between the pixel columns down to a few micrometers, which would result in very high fill factors. Future processes should either use more sophisticated mask technology in combination with projection lithography or mask-free photolithographic techniques such as direct laser writing.

4. Experimental

The general synthesis of the electroluminescent polymers has been described elsewhere [27]. The polymers were dissolved in toluene (10 mg mL^{-1}) and mixed with 0.2–0.5 wt % of the photoacid (**8**).

4-Octyloxydiphenyliodonium hexafluoroantimonate (OPPI) was purchased from Organica. For the process development, 60–100 nm thick films were spin-coated onto glass substrates under strict red-light conditions to prevent uncontrolled crosslinking of the films. The films were exposed to the broad UV spectrum of a 200 W high-pressure mercury lamp in a Süss Microtech mask aligner and subsequently soft-cured at 90 °C (**RX**), 85 °C (**GX**), and 75 °C (**BX**) for 1 min. Rinsing with tetrahydrofuran (THF) dissolved the unexposed parts of the film. Note that the whole lithography process was done in air.

The ITO anode lines were fabricated by conventional photolithography using homogeneously ITO-covered soda-lime glass purchased from Merck (Darmstadt). After photolithographic structuring, the substrates were thoroughly cleaned in chloroform, acetone, mucasol, and water and then exposed to ozone treatment for 20 min. A homogenous layer of PEDOT:PSS (Baytron PAL4083) was spin-coated under clean-room conditions and heated to 110 °C for 1 min to remove residual water. The substrates were transferred to a nitrogen glovebox for spin-coating and crosslinking of a hole-transport layer (HTL). The electroluminescent polymers were spin-coated on top as described above. Finally the substrates were post-cured for 15 min at 200 °C under a nitrogen atmosphere and subsequently transferred to a high-vacuum chamber (10^{-6} mbar (1 bar = 100 000 Pa)) for evaporation of the cathode (consisting of 4 nm barium covered by 150 nm silver) through a shadow mask.

The device characterization was done first with a Keithley 2400 source meter, a calibrated photodiode, and an Ocean Optics SD2000 CCD spectrometer. Subsequently, the devices were tested in the passive matrix operation mode with the OC2 evaluation board from Fraunhofer IPMS (Dresden).

Received: July 21, 2006
Revised: September 26, 2006

[1] S. R. Forrest, *Nature* **2004**, *428*, 911.
[2] A. Misra, P. Kumar, M. N. Kamalasanan, S. Chandra, *Semicond. Sci. Technol.* **2006**, *21*, R35.
[3] B. W. d'Andrade, S. R. Forrest, *Adv. Mater.* **2004**, *16*, 1585.
[4] S. R. Forrest, *Chem. Rev.* **1997**, *97*, 1793.
[5] M. Shtein, H. F. Gossenberger, J. B. Benziger, S. R. Forrest, *J. Appl. Phys.* **2001**, *89*, 1470.
[6] X. H. Yang, D. C. Muller, D. Neher, K. Meerholz, *Adv. Mater.* **2006**, *18*, 948.
[7] J. S. Kim, R. H. Friend, I. Grizzi, J. H. Burroughes, *Appl. Phys. Lett.* **2005**, *87*, 23 506.
[8] W. Su, D. Poplavskyy, F. So, H. Clearfield, D. Welsh, W. Wu, *Dig. Tech. Pap.-Soc. Inf. Disp. Int. Symp.* **2005**, *36*, 1871.
[9] J. Q. Ding, J. Gao, Y. X. Cheng, Z. Y. Xie, L. X. Wang, D. G. Ma, X. B. Jing, F. S. Wang, *Adv. Funct. Mater.* **2006**, *16*, 575.
[10] B. Liang, C. Y. Jiang, Z. Chen, X. J. Zhang, H. H. Shi, Y. Cao, *J. Mater. Chem.* **2006**, *16*, 1281.
[11] J. H. Choi, K. H. Kim, S. J. Choi, H. H. Lee, *Nanotechnology* **2006**, *17*, 2246.
[12] N. C. van der Vaart, H. Lifka, F. P. M. Budzelaar, J. E. J. M. Rubingh, *Dig. Tech. Pap.-Soc. Inf. Disp. Int. Symp.* **2004**, *35*, 1284.
[13] J. Birnstock, J. Blassing, A. Hunze, M. Scheffel, M. Stossel, K. Heuser, G. Wittmann, J. Worle, A. Winnacker, *Appl. Phys. Lett.* **2001**, *78*, 3905.
[14] C. MacPherson, M. Anzlowar, J. Innocenzo, D. Kolosov, W. Lehr, M. O'Regan, P. Sant, M. Stainer, S. Sysavat, S. Venkatesh, *Dig. Tech. Pap.-Soc. Inf. Disp. Int. Symp.* **2003**, *34*, 1191.
[15] D. G. Lidzey, M. A. Pate, M. S. Weaver, T. A. Fisher, D. D. C. Bradley, *Synth. Met.* **1996**, *82*, 141.

[16] T. Tachikawa, I. Norihito, S. Handa, D. Aoki, T. Miyake, *Dig. Tech. Pap.-Soc. Inf. Disp. Int. Symp.* **2005**, *36*, *1280*.
[17] C. C. Wu, J. C. Sturm, R. A. Register, M. E. Thompson, *Appl. Phys. Lett.* **1996**, *69*, 3117.
[18] G. B. Blanchet, Y. L. Loo, J. A. Rogers, F. Gao, C. R. Fincher, *Appl. Phys. Lett.* **2003**, *82*, 463.
[19] M. C. Suh, B. D. Chin, M. H. Kim, T. M. Kang, S. T. Lee, *Adv. Mater.* **2003**, *15*, 1254.
[20] M. Kashiwabara, K. Hanawa, R. Rasaki, I. Kobori, R. Matsuura, H. Yamada, T. Yamamoto, A. Ozawa, Y. Sato, S. Terada, J. Yamada, T. Sasaoka, S. Tamura, T. Urabe, *Dig. Tech. Pap.-Soc. Inf. Disp. Int. Symp.* **2004**, *35*, 1017.
[21] A. R. Duggal, J. J. Shiang, C. M. Heller, D. F. Foust, *Appl. Phys. Lett.* **2002**, *80*, 3470.
[22] J. S. Huang, G. Li, E. Wu, Q. F. Xu, Y. Yang, *Adv. Mater.* **2006**, *18*, 114.
[23] X. Gong, S. Wang, D. Moses, G. C. Bazan, A. J. Heeger, *Adv. Mater.* **2005**, *17*, 2053.
[24] J. Liu, Q. Zhou, Y. Cheng, Y. Geng, L. Wang, D. Ma, X. Jing, F. Wang, *Adv. Mater.* **2005**, *17*, 2974.
[25] C. D. Muller, T. Braig, H. G. Nothofer, M. Arnoldi, M. Gross, U. Scherf, O. Nuyken, K. Meerholz, *ChemPhysChem* **2000**, *1*, 207.
[26] M. S. Bayerl, T. Braig, O. Nuyken, C. D. Müller, M. Gross, K. Meerholz, *Macromol. Rapid Commun.* **1999**, *20*, 224.
[27] C. D. Müller, A. Falcou, N. Reckefuss, M. Rojahn, V. Wiederhirn, P. Rudati, H. Frohne, O. Nuyken, H. Becker, K. Meerholz, *Nature* **2003**, *421*, 829.
[28] E. Bacher, S. Jungermann, M. Rojahn, V. Wiederhirn, O. Nuyken, *Macromol. Rapid Commun.* **2004**, *25*, 1191.
[29] J. Lub, V. Recaj, L. Puig, P. Forcen, C. Luengo, *Liq. Cryst.* **2004**, *31*, 1627.
[30] B. M. I. van der Zande, S. J. Roosendaal, C. Doornkamp, J. Steenbakkers, J. Lub, *Adv. Funct. Mater.* **2006**, *16*, 791.
[31] K. Meerholz, C. D. Müller, O. Nuyken, in *Organic Light Emitting Devices* (Eds: K. Müllen, U. Scherf), Wiley-VCH, Weinheim, Germany **2005**.
[32] S. C. Graham, S. Fung, S. C. Moratti, R. H. Friend, *Synth. Met.* **1999**, *102*, 1169.
[33] S. A. VanSlyke, C. H. Chen, C. W. Tang, *Appl. Phys. Lett.* **1996**, *69*, 2160.
[34] U. Vogel, G. Bunk, A. Heinig, W. Jeroch, H. J. Holland, J. Amelung, in *ITG-Fachbericht Proceedings, Disp. and Vac. Electron.*, VDE, Berlin **2004**, p. 107.
[35] B. W. d'Andrade, V. Adamovich, R. Hewitt, M. Hack, J. J. Brown, *Proc. SPIE-Int. Soc. Opt. Eng.* **2005**, *5937*, 87.